Plasmodium berghei EXP-1 interacts with host Apolipoprotein H during *Plasmodium* liver-stage development

Cláudia Sá e Cunha[a,1], Britta Nyboer[b,1], Kirsten Heiss[b,c], Margarida Sanches-Vaz[a], Diana Fontinha[a], Ellen Wiedtke[d,e], Dirk Grimm[c,d,e], Jude Marek Przyborski[f], Maria M. Mota[a], Miguel Prudêncio[a,2], and Ann-Kristin Mueller[b,c,2]

[a]Instituto de Medicina Molecular, Faculdade de Medicina, Universidade de Lisboa, 1649-028 Lisboa, Portugal; [b]Parasitology Unit, Centre for Infectious Diseases, Heidelberg University Hospital, D 69120 Heidelberg, Germany; [c]German Centre for Infection Research, D 69120 Heidelberg, Germany; [d]Centre for Infectious Diseases, Virology, Heidelberg University Hospital, D 69120 Heidelberg, Germany; [e]BioQuant Institute, University of Heidelberg, D 69120 Heidelberg, Germany; and [f]Department of Parasitology, Faculty of Biology, Philipps University Marburg, D 35043 Marburg, Germany

Edited by Louis H. Miller, NIH, Rockville, MD, and approved December 29, 2016 (received for review April 22, 2016)

The first, obligatory replication phase of malaria parasite infections is characterized by rapid expansion and differentiation of single parasites in liver cells, resulting in the formation and release of thousands of invasive merozoites into the bloodstream. Hepatic *Plasmodium* development occurs inside a specialized membranous compartment termed the parasitophorous vacuole (PV). Here, we show that, during the parasite's hepatic replication, the C-terminal region of the parasitic PV membrane protein exported protein 1 (EXP-1) binds to host Apolipoprotein H (ApoH) and that this molecular interaction plays a pivotal role for successful *Plasmodium* liver-stage development. Expression of a truncated EXP-1 protein, missing the specific ApoH interaction site, or down-regulation of ApoH expression in either hepatic cells or mouse livers by RNA interference resulted in impaired intrahepatic development. Furthermore, infection of mice with sporozoites expressing a truncated version of EXP-1 resulted in both a significant reduction of liver burden and delayed blood-stage patency, leading to a disease outcome different from that generally induced by infection with wild-type parasites. This study identifies a host–parasite protein interaction during the hepatic stage of infection by *Plasmodium* parasites. The identification of such vital interactions may hold potential toward the development of novel malaria prevention strategies.

malaria | *Plasmodium* liver stages | host–parasite interaction | ApoH | EXP-1

Malaria remains the most important vector-borne disease worldwide, leading to particular devastation in sub-Saharan Africa. Malaria pathology is caused by the blood stages of single-celled parasites of the genus *Plasmodium*. However, before the symptomatic infection of red blood cells, *Plasmodium* parasites undergo an obligatory and clinically silent developmental phase in the liver, which constitutes an ideal target for disease prevention (1, 2). The liver stage of *Plasmodium* infection occurs after sporozoites are injected into the skin of the mammalian host upon a blood meal of an infected female *Anopheles* mosquito (3). Injected sporozoites eventually reach the liver, where they undergo a dramatic transition to form invasive first-generation merozoites that are released into the bloodstream. Hepatic *Plasmodium* infection comprises distinct developmental phases. After successful penetration of the endothelial barrier in the liver sinusoid (4) and traversal of several liver cells (5), the infectious sporozoite eventually invades a hepatocyte with the formation of a membranous replication-competent niche, the parasitophorous vacuole (PV) (6). The intracellular parasite then transforms into round exoerythrocytic forms (EEFs), which undergo repeated closed mitosis, ultimately leading to the formation of several thousand progenies. This development is exceptional for an obligate eukaryotic intracellular pathogen and likely depends on the extensive acquisition of lipids and nutrients from its host cell, while also relying on the parasite's own metabolism to ensure its survival and replication within host cells (7, 8).

Despite being metabolically active itself, the parasite has been shown to scavenge a plethora of host-cell molecules, such as glucose, cholesterol, fatty acids, phosphatidylcholine, or lipoic acids (8–12). Because *Plasmodium* parasites do not reside freely in the host cell cytoplasm or in endocytic compartments, but, rather, inside a vacuole formed de novo during the active invasion process, required nutrients have to cross the parasite plasma membrane as well as the PV membrane (PVM).

It is generally suggested that the PVM is central to nutrient acquisition, host-cell remodeling, waste disposal, environmental sensing, and protection of the intracellular pathogen from innate immune defenses (13). However, little is known about intrahepatic *Plasmodium* stages with regard to interactions between the parasite and the host hepatocyte and their potential for nutrient uptake and/or exchange. Small molecules (up to 800 Da) can cross the PVM freely via specialized transport channels (14), whereas larger molecules might reach the parasite via association and possibly fusion of late endosomes, lysosomes, or amphisomes with the PVM (15–19).

Several PVM-resident proteins have been identified, the largest family being the early transcribed membrane proteins (ETRAMPs), of which seven are present in the rodent malaria parasite *P. berghei* (*Pb*) (20). The most prominent members of this family, named up-regulated in infective sporozoites (UIS) 3 and 4, are expressed exclusively in sporozoites and liver stages (21, 22). Depletion of these proteins leads to developmental

Significance

The clinically silent intracellular development of *Plasmodium* parasites in the host liver is a prerequisite for the onset of malaria pathology. Liver stages can be completely eliminated by sterilizing immune responses and are promising targets for urgently needed antimalarial drugs and/or vaccines. The parasite is separated from the host cell cytoplasm by a parasitophorous vacuole (PV). We show that the PV membrane protein exported protein 1 interacts specifically with host Apolipoprotein H. The characterization of this protein–protein interaction revealed an essential role for both molecular partners during intrahepatic parasite growth. Our results improve our understanding of cell-biological aspects of host–pathogen interactions and may also help to develop new strategies to control *Plasmodium* infections.

Author contributions: D.G., M.M.M., M.P., and A.-K.M. designed research; C.S.e.C., B.N., K.H., M.S.-V., D.F., E.W., and J.M.P. performed research; E.W., D.G., and J.M.P. contributed new reagents/analytic tools; C.S.e.C., B.N., K.H., M.S.-V., D.F., D.G., J.M.P., M.P., and A.-K.M. analyzed data; and B.N., K.H., M.S.-V., D.F., M.P., and A.-K.M. wrote the paper.

The authors declare no conflict of interest.

This article is a PNAS Direct Submission.

[1]C.S.e.C. and B.N. contributed equally to this work.

[2]To whom correspondence may be addressed. Email: ann-kristin.mueller@uni-heidelberg.de or mprudencio@medicina.ulisboa.pt.

This article contains supporting information online at www.pnas.org/lookup/suppl/doi:10.1073/pnas.1606419114/-/DCSupplemental.

liver-stage arrest, and UIS3 was shown to interact with the host hepatocyte protein liver fatty acid binding protein 1 (LFABP1), suggesting a role in fatty acid scavenging during *Plasmodium* hepatic infection (23–25). Although another two ETRAMPs of the human malaria parasite, *P. falciparum* (*Pf*), are known to bind host-cell proteins, the function of these protein–protein interactions and that of most PVM-resident proteins remains largely elusive (26, 27).

Exported protein 1 (EXP-1) was the first protein described to associate with the PVM (28). It harbors a classical N-terminal signal peptide, and, upon trafficking via the endoplasmic reticulum–Golgi transport route, is inserted with its transmembrane domain into the PVM of both blood and liver parasite stages (29–33). It was shown later that the protein's N-terminal region faces the PV lumen, whereas its C terminus (CT) extends into the host-cell cytosol (34, 35). The same membrane topology was reported for other small PVM-resident proteins of the ETRAMP family, which are, together with EXP-1, organized in nonoverlapping oligomeric arrays within the PVM (36, 37). Because EXP-1 was found to be continuously trafficked to the PVM throughout at least the first half of liver-stage development, there was speculation as to whether the protein might also be trafficked back from the PVM to the PV or even the parasite cytosol (38). *Pf*EXP-1 is one of the most abundantly transcribed loci during ring and early trophozoite-stage development; it is therefore not surprising that it seems to exert vital functions during blood-stage development and was shown to be refractory to gene deletion (39–41). Recently, EXP-1 was predicted to possess GST activity, and it was demonstrated to conjugate glutathione onto hematin in vitro (42). Whether EXP-1 also exerts GST activity during *Plasmodium* intrahepatic development remains to be investigated.

Because recruitment of host-cell proteins to the parasite–host interface during liver-stage development could be a possible function for a PVM-resident protein such as EXP-1, we aimed at identifying potential host-cell interaction partners of this protein. We found that the C-terminal portion of *Pb*EXP-1 specifically interacts with host Apolipoprotein H (ApoH) and that this interaction is pivotal for successful liver-stage development of the parasite, both in vitro and in vivo. Our data suggest that *Plasmodium* liver stages use EXP-1 to specifically recruit host–hepatocyte ApoH to the parasite–host interface and to potentially mediate uptake of ApoH and/or ApoH-associated proteins or lipids.

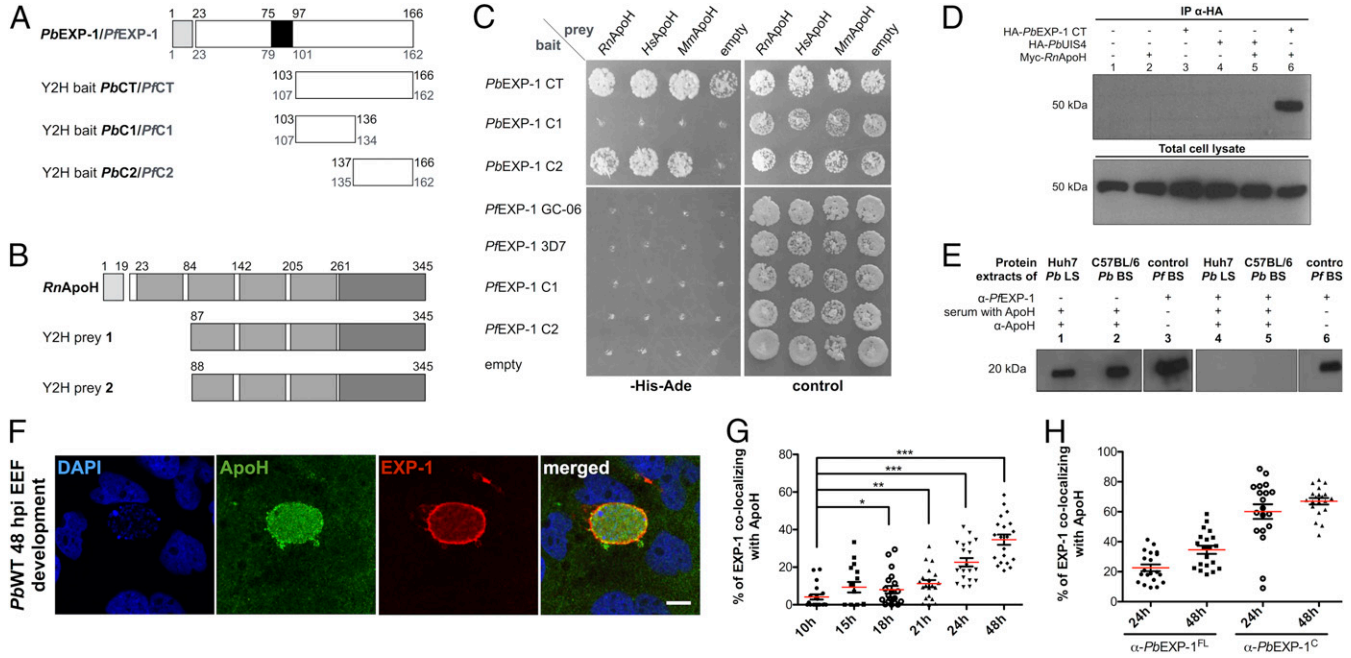

Fig. 1. EXP-1 CT interacts with host cell ApoH. (*A*) Primary structures of *Pb*EXP-1 and *Pf*EXP-1 with signal peptide (light gray box) and transmembrane domain (black box). C-terminal fragments CT, C1, and C2 used as baits in the Y2H screening and cotransformation experiments are shown below. (*B*) Primary structure of *Rn*ApoH with signal peptide (light gray box), CCP (gray), and Sushi-2 (dark gray) domains. Two prey cDNA sequences (Y2H prey 1 and 2) of rat ApoH were identified in the Y2H screening, and the corresponding protein fragments are shown. (*C*) *Pb*EXP-1 CT and C2 fragments interact with ApoH of rat, human, or mouse origin, whereas the C-terminal domain of *P. falciparum* EXP-1 did not interact with rat, human, or mouse ApoH, as demonstrated by yeast cotransformation assays. (*D*) HA-tagged *Pb*EXP-1 CT (HA-*Pb*EXP-1 CT) was immunoprecipitated by using an anti-HA antibody (Sigma, H9658), followed by immunoblotting with an anti-ApoH antibody (Abcam, ab108348). HEK293T cells were transfected with plasmids expressing HA-*Pb*EXP-1 CT, HA-tagged *Pb*UIS4 (HA-*Pb*UIS4), and Myc-*Rn*ApoH in various combinations. The ApoH–EXP-1 complex was pulled down in cells cotransfected with plasmids expressing both *Pb*EXP-1 CT and *Rn*ApoH (lane 6). No interaction was observed between *Pb*UIS4 and *Rn*ApoH (lane 5). (*E*) Far Western blot analysis and antibody inhibition assay of rat ApoH binding to EXP-1. Protein extracts of liver stages derived from *Pb*-infected Huh7 cells (lane 1) and of blood stages from *Pb*-infected mouse erythrocytes (lane 2) were separated by SDS/PAGE and blotted onto a nitrocellulose membrane, followed by incubation with ApoH-containing rat serum and ApoH detection with an anti-ApoH antibody. A band corresponding to ApoH was detected at the expected location of EXP-1 (~20 kDa), as confirmed by the similarly treated extracts of *Pf*-infected human erythrocytes (lane 3) and detection with an anti–*Pf*EXP-1 antibody. Incubation of the blots as described above with an anti–EXP-1 antibody before incubation with ApoH-containing rat serum rendered EXP-1 inaccessible to ApoH binding (lanes 4–6). (*F*) Immunofluorescence microscopy analysis of ApoH-stained (green) and EXP-1–stained (red) stained WT *Pb* parasites 48 hpi of Huh7 cells shows partial EXP-1 colocalization with ApoH and uptake of host ApoH into the parasite. (Scale bar: 10 μm.) (*G*) Quantification of EXP-1 colocalization with ApoH measured at various time points of liver-stage development using an anti-ApoH and an anti–EXP-1 antibody raised against full-length *Pb*EXP-1 (anti–*Pb*EXP-1^{FL}). Each symbol represents one parasite ($n = 20$, except for 15 h, where $n = 15$). *$P < 0.05$; **$P < 0.01$; ***$P < 0.001$ (unpaired t test). (*H*) Quantification of EXP-1 colocalization with ApoH at 24 and 48 hpi using an anti-ApoH antibody and either the anti–*Pb*EXP-1^{FL} or the anti–*Pb*EXP-1^{C} antibody, which exclusively detects the C-terminal region of EXP-1. Each symbol represents one parasite ($n = 20$). For *G* and *H*, data are shown as mean (indicated by red line) ± SD.

Results

PbEXP-1 Interacts with Rn ApoH. To address the functionality of *Pb*EXP-1 (PBANKA_0926700) during *Plasmodium* intrahepatic development, we carried out a yeast two-hybrid (Y2H) screen to identify novel host-cell molecular partners of this parasite protein. *Plasmodium* EXP-1 is a small, single-pass transmembrane protein with a classical signal peptide at its N-terminal portion (Fig. 1*A*), which localizes to the PVM (34, 37). Because EXP-1 CT is known to be exposed to the host cell cytoplasm (Fig. S1 *A*–*C*) (34, 35), this portion of the protein was used as bait in a Y2H screen against a *Rattus norvegicus* (*Rn*) hepatocyte cDNA library. The screen identified several putative interacting partners of EXP-1, with rat ApoH (*Rn*ApoH; NP_001009626.1), also known as beta-2-glycoprotein I (Fig. 1*B*), emerging as the most frequent hit (Table S1).

Next, we performed direct interaction assays to confirm the interaction with rat ApoH and to identify the portion of the EXP-1 CT responsible for the interaction. To this end, cotransformation experiments were conducted (Fig. 1*C*), by using the complete CT of *Pb*EXP-1 (amino acids 103–166), as well as fragments corresponding to the *Pb*EXP-1 amino acids 103–136 (C1 region) and 137–166 (C2 region), as bait proteins (Fig. 1*A*). *Rn*, *Mus musculus* (*Mm*; NP_038503.4), and *Homo sapiens* (*Hs*; NP_000033.2) ApoH were used as preys in these Y2H assays (Fig. 1*C*). Our results not only confirmed the interaction between *Pb*EXP-1 and ApoH of rat, mouse, and human origin, but further identified the C2 region of *Pb*EXP-1 as responsible for this interaction (Fig. 1*C*).

Similar to the studies with *Pb*EXP-1, we used the complete CT of *Pf*EXP-1 (amino acids 107–162) of the strains 3D7 and GC-06, which represent the two different naturally occurring variants of the protein that differ only at position 136 (31), as bait proteins. Alternatively, we used fragments of *Pf*EXP-1 3D7 corresponding to amino acids 107–134 and 135–162 (C1 and C2 region, respectively) (Fig. 1*A*). In contrast, *Pf*EXP-1 (PF3D7_1121600) CT differs substantially from its *Pb*EXP-1 ortholog (Fig. S1*D*), and indeed, when performing direct interaction assays using different *Pf*EXP-1 CT variants (Fig. 1*A*), no interaction with ApoH of rat, mouse, or human origin could be detected in three independent experiments (Fig. 1*C* and Table S2).

The *Pb*EXP-1 and *Rn*ApoH protein–protein interaction was further confirmed by coimmunoprecipitation studies using an HA-tagged version of the C-terminal region of *Pb*EXP-1 (HA-*Pb*EXP-1 CT) and Myc-tagged *Rn*ApoH (Myc-*Rn*ApoH). In these experiments, the complex was successfully pulled down with two independent α-HA antibodies and detected by immunostaining with either α-Myc (Fig. S2*A*) or α-ApoH antibodies (Fig. 1*D*), respectively. No interaction with *Rn*ApoH was observed with HA-tagged *Pb*UIS4 (HA-*Pb*UIS4), used as a control in these experiments (Fig. 1*D*). The interaction between *Pb*EXP-1 and *Rn*ApoH was further validated by far Western blot and antibody inhibition assays. In these experiments, protein extracts of *Pb*-infected Huh7 cells or *Pb*-infected C57BL/6 mouse blood were separated by SDS/PAGE and blotted onto a nitrocellulose membrane that was subsequently incubated with ApoH-containing rat serum and washed to remove any unspecific bound proteins. Binding of ApoH to EXP-1 was demonstrated by staining with an α-ApoH antibody, which revealed a band of ∼20 kDa, corresponding to the size of the *Pb*EXP-1 protein (Fig. 1*E*). Detection of *Pf*EXP-1 in *Pf* blood-stage cultures with α-*Pf*EXP-1 antibody, which we have shown to be fully reactive against the *Pb*EXP-1 protein (Fig. S2*B*), was used as control (Fig. 1*E*). Incubation of the membrane with α-*Pf*EXP-1 antibody, which was raised against the protein's CT, before incubation with rat serum completely blocked binding of ApoH, again confirming the specificity of the interaction (Fig. 1*E*). Moreover, we carried out ELISAs where wells coated with recombinant *Rn*ApoH were incubated or not with lysates of *Pb*-infected or noninfected Huh7 cells, followed by washing and incubation with an α-*Pb*EXP-1 antibody. Our results showed a clear increase in the signal detected only in samples incubated with lysates of *Pb*-infected cells, solidifying the interaction between *Pb*EXP-1 and *Rn*ApoH (Fig. S2*C*). Immunofluorescence microscopy colocalization studies were conducted from 10 to 48 h postinfection (hpi) by using a commercial α-ApoH antibody and an α-*Pb*EXP-1 antibody (Fig. 1*F*). Our results showed that the two proteins colocalize in the PVM region of the parasite. Interestingly, colocalization of ApoH and EXP-1 increased during EEF development, with, on average, 40% of the total EXP-1 signal in EEFs analyzed at 48 hpi colocalizing with ApoH (Fig. 1*G*). Finally, we performed colocalization studies 24 and 48 hpi using antibodies specifically raised against the full-length *Pb*EXP-1 (*Pb*EXP-1^{FL}) or against its C-terminal regions (*Pb*EXP-1^{c}, raised against amino acids 103–166; see also Fig. 1*A*) of *Pb*EXP-1 (Fig. 1*H*). These results clearly confirm the colocalization of ApoH with the C-terminal domain of EXP-1 facing the hepatocyte cytoplasm. Overall, our data demonstrated, by a variety of independent methods, a parasite–host molecular interaction between the *Pb*EXP-1 and *Rn*ApoH proteins, prompting further investigation of the physiological role of this interaction during hepatic infection by *Plasmodium* parasites.

ApoH Plays an Important Role in Hepatic Infection by *Plasmodium* Parasites. We next used RNA interference (RNAi) to specifically silence the expression of the gene encoding endogenous ApoH to examine both the biological and physiological relevance of this particular parasite–host interaction for intrahepatic development of the parasite. To this end, the expression of ApoH in Huh7 cells was down-modulated by specific siRNA oligonucleotides (siRNAs ApoH_1–3; Fig. S3*A* and Table S3), and the resulting effect on infection by *Pb* sporozoites was analyzed comprehensively (43). First, RNAi-mediated knockdown of ApoH expression in hepatocytes was confirmed by quantitative real-time PCR (qRT-PCR) and Western blotting (Fig. S3 *A* and *B*, respectively) and shown to be stable over the 48-h period of infection (Fig. S3*C*). Because siRNA ApoH_1 showed the strongest phenotype, it was used in all experiments where a single siRNA was used. *Pb* infection of Huh7 cells after down-modulation of ApoH expression was then compared with that of control cells, transfected with scrambled siRNA (Neg siRNA). Initially, cells were infected with either luciferase-expressing or wild-type (WT) *Pb* sporozoites, and infection was measured by bioluminescence (44) or qRT-PCR, respectively (Fig. 2 *A* and *B*). Our results showed that down-modulation of ApoH expression leads to a significant decrease in overall infection (Fig. 2 *A* and *B*), which was not due to impaired invasion of sporozoites (Fig. S3*D*). We then used immunofluorescence microscopy to assess the effect of ApoH down-modulation on parasite numbers (Fig. 2*C*) and sizes (Fig. 2 *D* and *E*). A comparison of the resulting infection rates clearly showed that ApoH down-modulation results in a significant decrease in the development of *Plasmodium* liver stages (Fig. 2*D*). This finding suggests a specific requirement of host-cell ApoH for successful intrahepatic *Plasmodium* development.

To further assess the role of ApoH in an in vivo setting, ApoH expression was specifically down-regulated in livers of mice before they were infected with *Pb* parasites. To this end, we made use of recombinant adeno-associated viral (rAAV) particles of serotype 8, which exhibit a characteristic hepatotropism (45–48), to deliver anti-*Mm*ApoH–specific short hairpin RNAs (shRNAs) to the mouse livers. At 14 d after rAAV injection, mice were infected with *Pb* WT sporozoites. qRT-PCR measurements of the knockdown efficiency of anti-*Mm*ApoH shRNAs (176 and 725; Table S3) 42 hpi showed that both shRNAs significantly reduced ApoH expression levels in comparison with the control group that received no rAAV (Fig. 2*F*). Interestingly, injection of any rAAV elevated parasite liver load compared with the no-rAAV group, which only received the parasite injection (Fig. 2*G*). This effect seemed to be solely due to the presence of rAAVs, because parasite liver burden was also elevated in the empty vector control

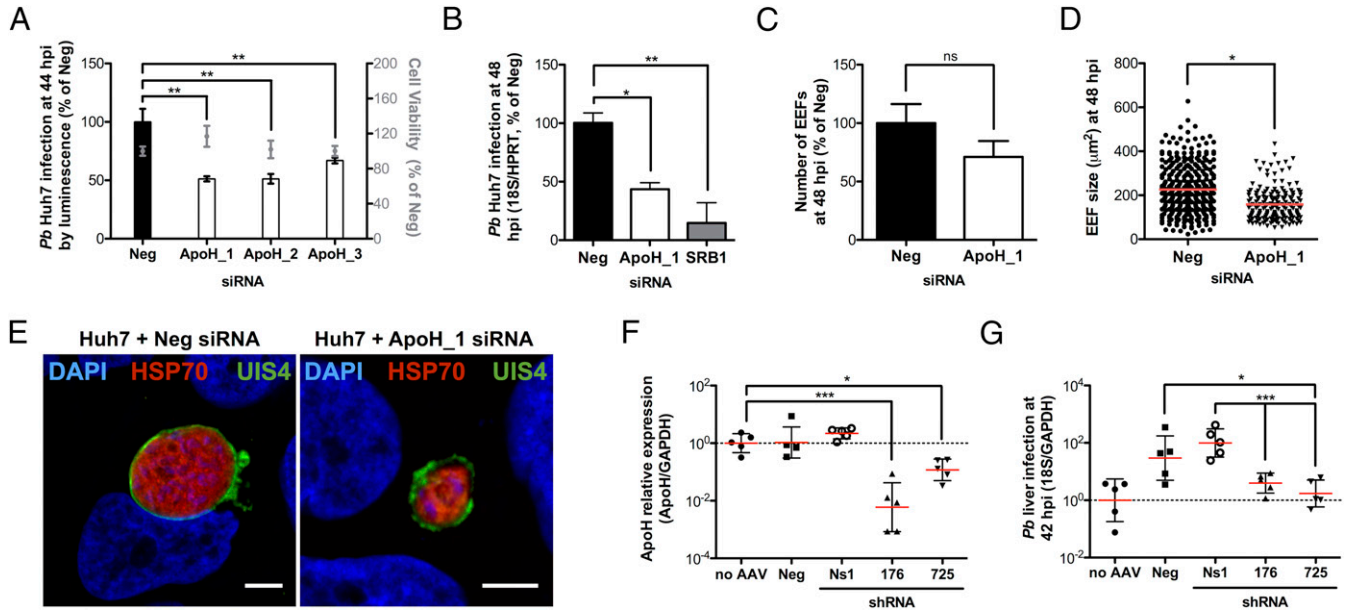

Fig. 2. Down-regulation of host ApoH severely impairs parasite development in vitro and in vivo. (*A*) Parasite load of Huh7 cells transfected with three anti-ApoH siRNAs (ApoH_1–3) and infected with luciferase-expressing *Pb* parasites, measured 44 hpi by luminescence. Results were normalized to the infection load of cells transfected with a scrambled siRNA (Neg) used as negative control. (*B*) Parasite load of Huh7 cells transfected with ApoH_1 siRNA and infected with WT *Pb* parasites measured 48 hpi by qRT-PCR. Results were normalized to the infection load of cells transfected with Neg siRNA (negative control). Cells transfected with a siRNA targeting the SRB1 gene (72) were used as positive controls. Human *HPRT* was used as a housekeeping gene. (*C*) EEF numbers in *Pb*-infected Huh7 cells previously transfected with ApoH_1 siRNA measured by immunofluorescence microscopy 48 hpi. Results were normalized to the number of EEFs in cells transfected with Neg siRNA (negative control). Three independent experiments were performed, and data from one representative experiment are shown in *A* and *B*. Data in *C* correspond to the pool of two independent experiments. (*D*) EEF sizes in *Pb*-infected Huh7 cells previously transfected with ApoH_1 siRNA ($n = 173$) measured by immunofluorescence microscopy 48 hpi. *Pb*-infected cells transfected with Neg siRNA ($n = 326$) were used as negative controls. Three independent experiments were performed, and data from one representative experiment are shown in *D*, where each symbol represents one parasite. For *A*–*D*: $*P < 0.05$; $**P < 0.01$ (Mann–Whitney test). ns, not significant. Data are shown as mean (in *D* indicated by red line) ± SD. (*E*) Representative images of *Pb* EEFs in Huh7 cells transfected with Neg siRNA or ApoH_1 siRNA at 48 hpi stained with anti-HSP70 (red) and anti-UIS4 (green) antibodies. Nuclei were stained with DAPI. (Scale bars: 10 μm.) (*F*) qRT-PCR analysis of ApoH expression in the livers of mice. Five C57BL/6 mice per group were i.v. injected with 5×10^{10} rAAV particles carrying different shRNA constructs and 14 d later infected with 10,000 *Pb* WT sporozoites. Forty-two hours after *Pb* infection, livers were isolated. The no-rAAV group received only the parasite injection. Results were normalized to the no-rAAV group, which was set to 1 (dotted line). Empty vector (Neg) and nonsilencing (Ns1) shRNAs were used as negative control; 176 and 725 are *MmApoH*-specific shRNAs. Mouse *GAPDH* was used as a housekeeping gene. (*G*) *Pb* liver infection in the same mice as in *F* was normalized to the no-rAAV group. All mice were age-matched. For *F* and *G*: $*P < 0.05$; $***P < 0.001$ (one-way ANOVA, Dunnett's multiple comparison test). Data are shown as mean (indicated by red line) ± SD. Each symbol represents one mouse ($n = 5$).

group (Neg), which did not encode any shRNA (Fig. 2*G*). Most importantly, parasite liver burden of mice injected with either anti-ApoH shRNA was significantly reduced compared with the non-silencing shRNA (Ns1) or empty vector control groups (Fig. 2*G*). Together, our results show that ApoH plays a crucial role during hepatic infection by *Pb* parasites, both in vitro and in vivo.

Truncation of the C2 Region of EXP-1 Impairs ApoH Colocalization and Internalization. Our data so far indicated that the host protein ApoH contributes to *Pb* development, presumably through its interaction with the C2 region of its interaction partner, EXP-1. Despite several attempts, a full knockout of *Pb*EXP-1 could not be obtained by using either conventional standard *Pb* transfection or PlasmoGEM (PbGEM_332867) vectors (Fig. S4 *A*–*D*) (49). Moreover, a promoter-exchange approach did not result in transgenic parasites, which would have expressed EXP-1 only during blood-stage and late liver-stage development (Fig. S4 *E* and *F*). Because our data using the yeast system highlighted the importance of the C2 region of EXP-1 for the interaction with ApoH (Fig. 1*C*), transgenic *Pb* parasite lines expressing a C2-truncated version of *Pb*EXP-1, *Pb*EXP-1ΔC2, were generated in both the *Pb* and *Pb*GFP-luc$_{con}$ parasites (clone 2 or clones 3 and 4, respectively) (Fig. 3*A*). Interestingly, even though EXP-1 appeared to be refractory to gene deletion because of its essentiality for the intraerythrocytic development, we were able to isolate this EXP-1 truncation mutant after successful transfection and limited dilution. The resulting *Pb*EXP-1ΔC2 parasites completed their life cycle indistinguishably from WT parasites up until and including hepatocyte invasion (Table S4). This result indicates that the carboxyl-terminal C2 part of EXP-1 is not essential for intraerythrocytic parasite development because we were able to generate deletion mutants lacking this particular portion of the PVM-resident protein. The characteristic movement of infectious sporozoites and their invasion capacity (Fig. S5 *A* and *B*) were also not impaired in the *Pb*EXP-1ΔC2 parasites. Additionally, immunofluorescence microscopy analysis of Huh7 cells infected with clonal *Pb*EXP-1ΔC2 lines and stained with antibodies against the PVM proteins UIS4 and EXP-1 indicated that neither the integrity of the vacuolar membrane nor the localization of EXP-1 were compromised in transgenic parasites (Fig. 3*B*). However, a significantly decreased colocalization of EXP-1 and ApoH was observed in additional immunofluorescence experiments using *Pb*EXP-1ΔC2–infected Huh7 cells, compared with WT *Pb*-infected cells (Fig. 3 *C* and *D*). Furthermore, quantification of accumulated ApoH in liver stages of *Pb*WT and *Pb*EXP-1ΔC2 parasites showed a significantly reduced uptake of ApoH in intrahepatic stages of parasites expressing the C-terminally truncated version of EXP-1 (Fig. 3*E*). This finding clearly suggests that the interaction between the two proteins is severely compromised when the C2 region of EXP-1 is truncated, in agreement with our data shown in Fig. 1. Additionally, it points to a hitherto-undescribed instance of an interaction between a *Plasmodium* protein at the PVM and a host protein, leading to the accumulation of the latter inside the parasite.

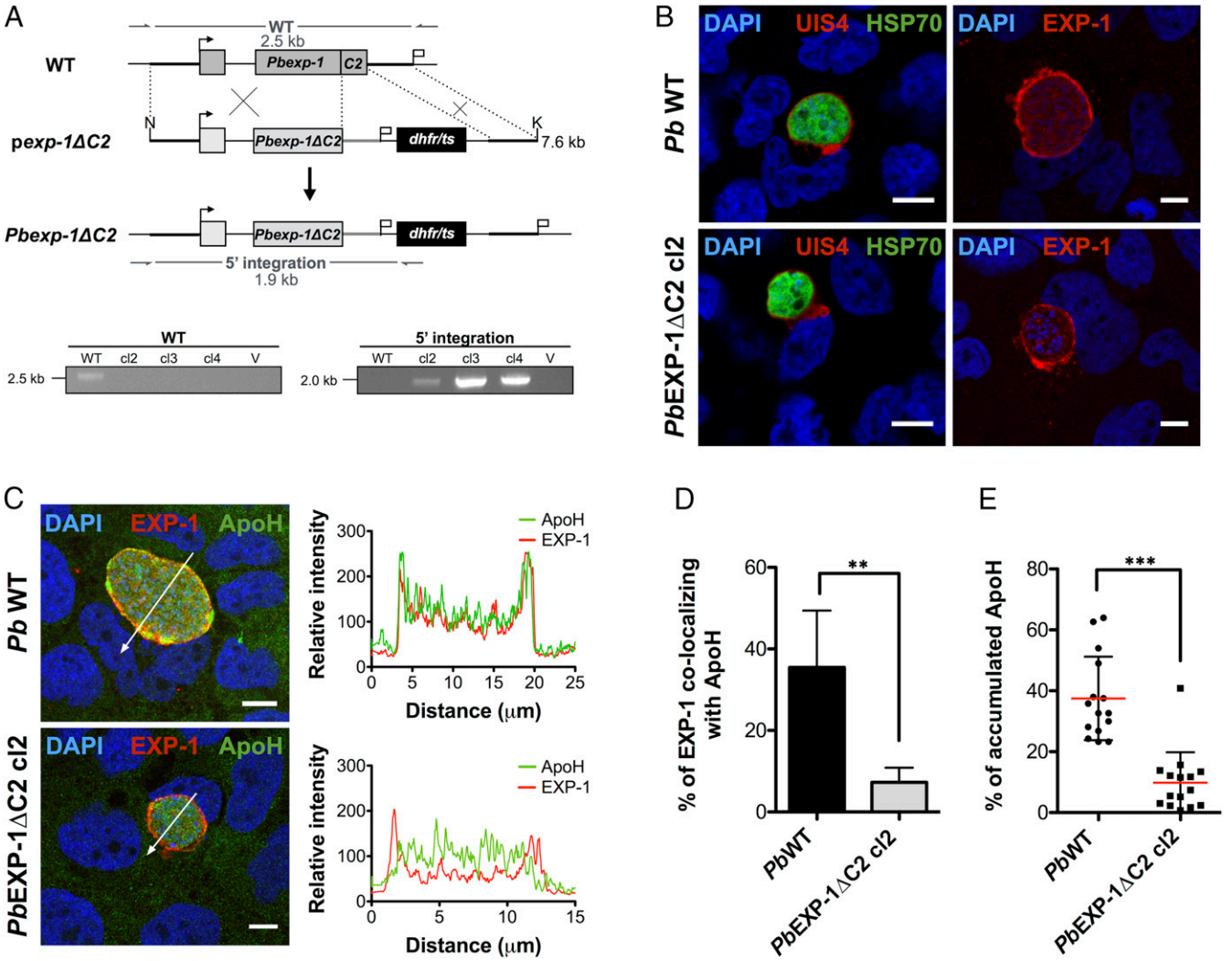

Fig. 3. Truncation of EXP-1 CT leads to both reduced ApoH colocalization and internalization. (*A*, *Upper*) Replacement strategy for generation of the *Pb*EXP-1 C2 deletion mutant (ΔC2). (*A*, *Lower*) Successful integration is shown for three clonal transgenic parasite lines (cl2 in *Pb*, cl3 and cl4 in *Pb*GFP-luc$_{con}$ background) generated in two independent transfections. Binding sites for primers used for genotyping are indicated by arrows. V, vector; WT, WT gDNA. (*B*) Immunofluorescence microscopy analysis of WT *Pb* and *Pb*EXP-1ΔC2 clone 2 liver stages 48 hpi. Parasite cytoplasm is stained with anti-HSP70 antibody (green), the PVM with anti-UIS4 or anti–EXP-1 antibodies (red), and nuclei with DAPI (blue). (Scale bars: 10 μm.) (*C*) Colocalization of parasite EXP-1 (red) and host ApoH (green) in WT and *Pb*EXP-1ΔC2 parasite lines. (*C*, *Left*) representative immunofluorescence microscopy images. (Scale bars: 10 μm.) (*C*, *Right*) Histograms showing the intensity of the red and green signals across the section indicated in the images in *C*, *Left*. (*D*) Quantification of EXP-1–ApoH colocalization. Colocalization was measured as percent of total EXP-1 that colocalizes with ApoH. (*E*) Accumulation of ApoH was measured for liver stages of WT and *Pb*EXP-1ΔC2 parasites. For *D* and *E*: $^{**}P < 0.01$; $^{***}P < 0.001$ (Mann–Whitney test). Two independent experiments were performed, and data from one experiment are shown as mean ± SD.

Truncation of the C2 Region of EXP-1 Impairs Intrahepatic *Plasmodium* Development. We next assessed whether deletion of the utmost CT of *Pb*EXP-1 (*Pb*EXP-1ΔC2) would equally result in a reduced intrahepatic development when the parasite binding partner is no longer able to interact with the host-cell factor ApoH at the parasite/host interface, hence presumably severing the liver-stage parasite from its exogenous nutrient supply. A detailed analysis of Huh7 cell infection by *Pb*EXP-1ΔC2 mutant lines showed that truncation of the EXP-1 C2 region leads to a phenotype similar to that observed when host ApoH expression was down-modulated by RNAi (Fig. 2 *C*–*E*). In fact, our analyses of infected Huh7 cells 48 h after sporozoite addition showed that infection with any of the three *Pb*EXP-1ΔC2 clones led to lower EEF numbers (Fig. 4*A*) and sizes (Fig. 4*B*) than those yielded by their counterparts containing full-length EXP-1. In addition, we generated a complementation parasite line (*Pb*EXP-1compl) by applying the same genetic strategy as for the *Pb*EXP-1ΔC2 transgenic line (Fig. S6*A*). The *Pb*EXP-1compl parasite displayed an integral vacuolar membrane with similar localizations for UIS4 and EXP-1 (Fig. S6*B*). Furthermore, its intrahepatic growth efficiency (Fig. S6 *C* and *D*) was comparable with that of *Pb* WT parasites, despite a currently unexplained small, yet significant, increase in EEF numbers of the *Pb*EXP-1compl parasite relative to the WT counterpart (Fig. S6*C*). The growth defect of *Pb*EXP-1ΔC2 parasites observed during intrahepatic development was further demonstrated by quantifying membrane-enclosed first-generation merozoites (merosome formation) in Huh7 cells. Our results indicate that merosome formation is clearly delayed in transgenic *Pb*EXP-1ΔC2 parasites compared with their WT parasite controls (Fig. S7*A*). This finding was shown by the significant difference in number of merosomes detected in the former compared with the latter at 65 hpi, which was no longer observed at the later, 72-hpi time point (Fig. S7*A*). Collectively, these results provide further support to the notion that the interaction between the C2 region of the parasite's EXP-1

protein and the host's ApoH molecule plays an important role during the hepatic stage of *Plasmodium* infection.

Impairment of the EXP-1/ApoH Interaction Leads to a Decrease in Liver Parasite Burden and in the Severity of Pathology. Having established that the truncation of the C2 region of EXP-1 leads to a decreased interaction with ApoH in vitro, we next investigated the in vivo infection of C57BL/6 mice by *Pb*EXP-1ΔC2 parasites. Again, similarly to what we observed when ApoH expression was down-modulated in vivo (Fig. 2*G*), our results showed a decrease in the liver parasite load of mice infected with either of the *Pb*EXP-1ΔC2 clones at 42 hpi, compared with their respective controls (Fig. 4*C*). Moreover, late intrahepatic development (72–96 hpi) was additionally significantly reduced in *Pb*EXP-1ΔC2 compared with WT infections (Fig. S7*B*). We then asked whether an impairment of the EXP-1/ApoH interaction would have any consequences in terms of disease severity. To evaluate this possibility, C57BL/6 mice were infected i.v. with 10,000 WT *Pb* or *Pb*EXP-1ΔC2 sporozoites, and infection was allowed to proceed to the blood stage. Daily monitoring of blood parasitemia (Fig. 4*D*), disease symptoms, and mouse survival showed a 1-d delay in the patency of blood-stage infection and a significantly increased survival of the mice infected with the transgenic parasites, compared with their WT counterparts (Table 1). Finally, we infected mice with 10^6 erythrocytic stages of both WT and *Pb*EXP-1ΔC2 parasites and followed the course of parasitemia. Our results showed that, when the intrahepatic phase of infection is bypassed, no significant differences are observed in the overall replication rates of the parasites in the blood (Fig. 4*E*).

These observations clearly indicate that the truncation of the region of the EXP-1 protein responsible for the interaction with ApoH has a significant impact solely during the intrahepatic stage of parasite development.

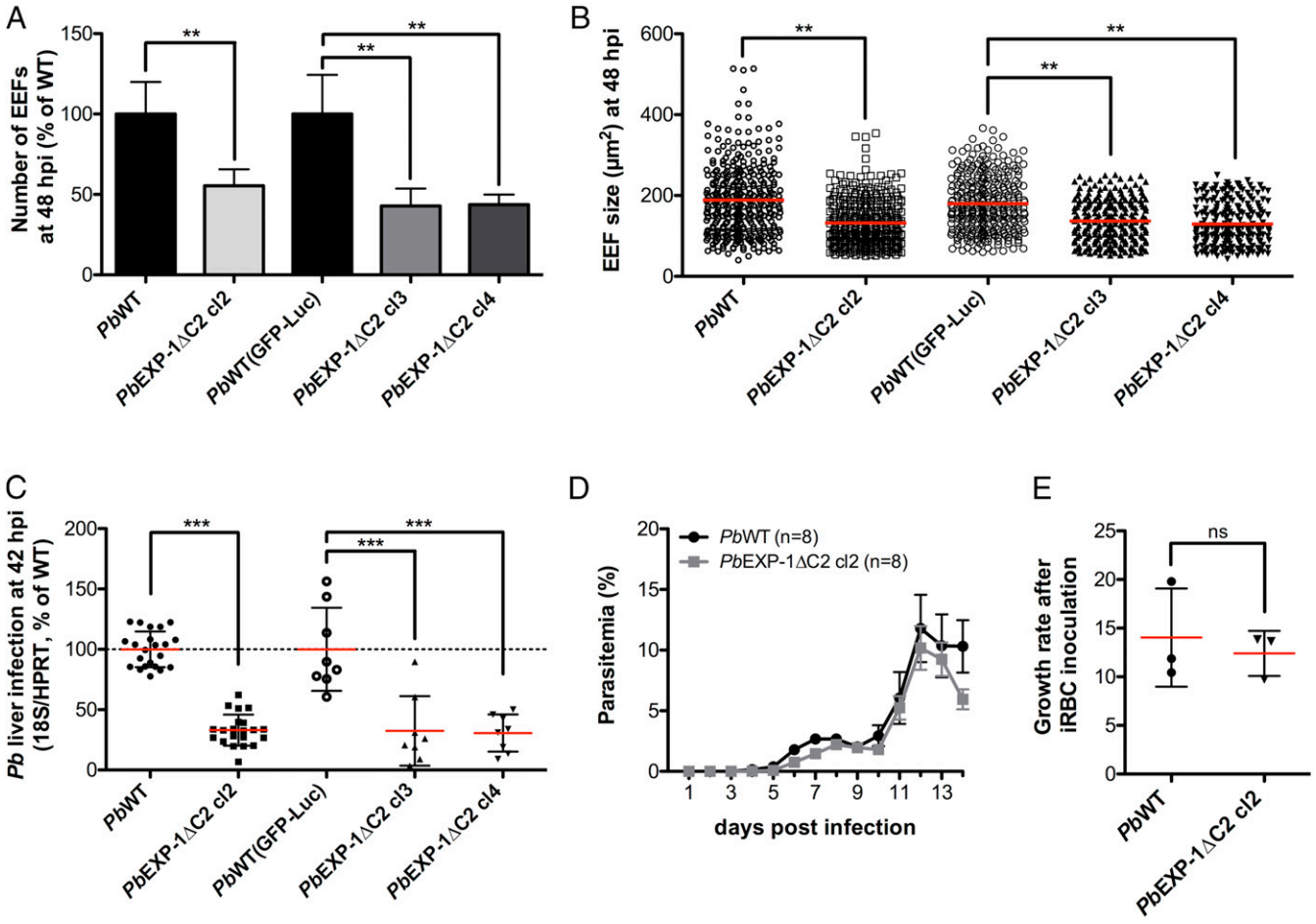

Fig. 4. Truncation of EXP-1 CT leads to impaired intrahepatic parasite development in vitro and decreased liver infection in vivo. (*A*) EEF numbers in Huh7 cells infected with three *Pb*EXP-1ΔC2 clonal transgenic parasite lines compared with their respective WT controls measured 48 hpi by immunofluorescence microscopy. Results were normalized to WT controls. Data from two independent experiments were pooled and are shown as mean ± SD. (*B*) EEF sizes in Huh7 cells infected with three *Pb*EXP-1ΔC2 clonal transgenic parasite lines compared with their respective WT controls measured 48 hpi by immunofluorescence microscopy (mean indicated by red line). Data from two independent experiments were pooled, and each symbol represents one parasite (*Pb*WT, $n = 350$; cl 2, $n = 362$; *Pb*WT (GFP-Luc$_{con}$), $n = 309$; cl 3, $n = 244$; cl 4, $n = 235$). (*C*) Parasite load in the livers of C57BL/6 mice infected with *Pb* WT or *Pb*EXP-1ΔC2 clonal lines measured by qRT-PCR 42 hpi after i.v. injection of 10,000 sporozoites. Parasite 18S rRNA expression was normalized to respective WT controls, which were set to 100% (dotted line). Mouse *HPRT* was used as the housekeeping gene. Data were pooled from five and two independent experiments for clone 2 and clones 3/4, respectively. Each symbol represents one mouse [*Pb*WT/cl 2, $n = 22$; *Pb*WT (GFP-Luc$_{con}$) clo 3/cl 4, $n = 8$]. (*D*) Mean parasitemia (±SEM) of female C57BL/6 mice after i.v. infection with 10,000 sporozoites from either WT or *Pb*EXP-1ΔC2 ($n = 8$). (*E*) Multiplication rates of WT and *Pb*EXP-1ΔC2 intraerythrocytic stages after inoculation of 10^6 infected red blood cells of each parasite line ($n = 3$). Growth rates of the two parasite lines were calculated daily and are shown as mean. No significant (ns) difference between WT and *Pb*EXP-1ΔC2 was detected. For *A*–*C* and *E*: Data are shown as mean ± SD. $^*P < 0.05$; $^{**}P < 0.01$; $^{***}P < 0.001$ (Mann–Whitney test).

Discussion

In this study, we identified a host–*Plasmodium* interaction between the parasitic PVM-resident protein *Pb*EXP-1 and host-cell ApoH and demonstrated its importance in facilitating the parasite's preerythrocytic development. EXP-1 belongs to a short list of parasite-derived proteins that have been shown to localize at the intrahepatic host–parasite interface, which includes LISP1/2, IBIS1, UIS3/4, and components of the PTEX translocon (23, 24, 33, 50–53). Although it was identified >30 y ago and is abundantly expressed during blood- and liver-stage parasite development (28, 32), the function of *Plasmodium* EXP-1 largely remained elusive. Recently, a study by Lisewski et al. suggested that in *Pf* erythrocytic stages, EXP-1 functions as a membrane GST, efficiently degrading cytotoxic hematin (42). Whether EXP-1 also acts as GST during intrahepatic development is not known. However, it is tempting to speculate that the GST function may be more important during the parasite's blood-stage development, when large amounts of toxic hematin are generated, whereas recruitment of host-cell nutrients might be more important during the extensive liver-stage replication phase. In fact, our study strongly suggests that EXP-1 plays distinct roles during the liver and blood stages of infection. As shown by our results with the *Pb*EXP-1ΔC2 parasite, the interaction of the EXP-1 CT with ApoH during the hepatic stage fulfills a function that is not essential for blood-stage parasite survival. So far, such a specific host–parasite interaction during intrahepatic development was only described for the UIS3 protein, which binds host LFABP (25). Interestingly, down-regulation of LFABP1 expression impairs liver-stage growth (25), similarly to what we observe when ApoH expression is silenced. However, unlike UIS3, EXP-1 is a cross-stage antigen and might also function as a binding partner for host proteins during erythrocytic development.

Our analysis of the subcellular localization of EXP-1 and ApoH showed not only that the two proteins colocalize in the PVM region, but also that ApoH appears to additionally accumulate inside the parasite. However, the mechanism by which ApoH enters the parasite and crosses both the PVM and the parasite's plasma membrane remains unknown. Interestingly, Hanson et al. recently reported that both known PVM-resident proteins, EXP-1 and UIS4, must be continuously exported to the PVM, at least during the first 30 h of intrahepatic development. This finding raises the possibility that these proteins may be trafficked back into the PV or even into the parasite's cytoplasm (38). If EXP-1 is indeed subjected to retrograde trafficking, it might serve as a shuttle protein for ApoH. An alternative entry route would be the PVM PTEX translocon, which is also expressed during liver-stage development (53). EXP-2 is hypothesized to form the membrane-spanning pore of the PTEX translocon and may have several functions apart from protein export, such as nutrient acquisition (53). It could thus present a potential import route for ApoH, with EXP-1 functioning as a bridging or recruiting molecule. Our results show that transgenic liver-stage parasites expressing a truncated EXP-1 protein exhibited decreased colocalization with ApoH at the PVM and, more importantly, decreased uptake of ApoH into the parasite's cytoplasm.

Our findings revealed an important role for ApoH during liver-stage, but not intraerythrocytic, *Plasmodium* development, because either reduced ApoH expression or expression of a truncated EXP-1 protein resulted in a significant decrease in parasite hepatic burden, both in vitro and in vivo. ApoH is an abundant plasma protein, which is mainly synthesized in the liver, but also in intestinal tissues and placenta cells (54–56). The protein comprises five repeats known as complement control protein (CCP) repeats, functioning as protein–protein interaction modules (57, 58). Although the first four repeats are structurally related, the fifth domain is more variable and contains, for example, a highly positively charged region and three, instead of two, disulfide bridges (56, 58). Several different functions have been assigned to human ApoH, such as clearing apoptotic bodies and microparticles from the circulation, interacting with oxidized LDL, or scavenging toxic compounds as well as cellular debris (59, 60). Because ApoH is responsible for the clearance of plasma liposomes, which also contain, for example, cholesterols (61), it is tempting to speculate that ApoH might transport lipids and/or cholesterols to the intracellular parasite via its direct interaction with *Plasmodium* EXP-1, allowing for successful intrahepatic development of the parasite. This speculation raises the additional possibility that the interaction of EXP-1 with ApoH might also serve to internalize the latter and/or provide the parasite with ApoH molecular partners.

In conclusion, our data highlight the importance of the ApoH/EXP-1 interaction for successful liver-stage *Plasmodium* development and contribute to our understanding of how the PVM serves as a platform for host–parasite interactions. Based on our findings, we propose that other PVM family members may also engage in specific protein interactions with host-cell proteins and thereby serve as docking proteins for important host-cell factors. Interference with such crucial parasite–host interactions may strengthen the search for innovative intervention strategies against malaria.

Materials and Methods

See additional materials and methods in *SI Materials and Methods*.

Ethics Statement. All animal experiments were performed according to European regulations concerning Federation for Laboratory Animal Science Associations category B and Society of Laboratory Animal Science standard guidelines. Animal experiments were approved by German authorities (Regierungspräsidium Karlsruhe), § 8 Abs. 1 Tierschutzgesetz (TierSchG) under the license G-260/12 and by the internal animal care committee of the Instituto de Medicina Molecular and were performed according to national and European regulations. For all experiments, female C57BL/6 and outbred NMRI mice were purchased from Janvier or Charles River Breeding Laboratories, and male inbred C57BL/6J mice were purchased from Charles River Breeding Laboratories. All mice were kept under specific pathogen-free conditions within the animal facility at Heidelberg University [Interfakultäre Biomedizinische Forschungseinrichtung (IBF)] and the facilities of the Instituto de Medicina Molecular, Lisbon, respectively.

Table 1. Prepatent period of C57BL/6 mice infected with 10,000 *Pb*EXP-1ΔC2 sporozoites is prolonged and results in increased survival rates compared with WT controls

Parasite strain	Prepatent period, *	*P* value (clone vs. WT control)†	No. of surviving/no. of infected animals	*P* value (clone vs. WT control)†
*Pb*WT	3.7	—	3/8	—
*Pb*EXP-1 ΔC2 cl2	4.7	0.0027	7/8	0.0359
*Pb*GFP-luc$_{con}$ WT	3.3	—	3/8	—
*Pb*GFP-luc$_{con}$EXP-1ΔC2 cl3	4.9	0.0002	8/8	0.0359
*Pb*GFP-luc$_{con}$EXP-1ΔC2 cl4	4.7	0.0018	7/7	0.4385

*Number of days after sporozoite inoculation until infected erythrocytes were detected in blood smear examination.
†Statistical analysis was performed by using the log-rank (Mantel–Cox) test with GraphPad Prism.

Cell Culture. Huh7 cells, a human hepatoma cell line (a gift from Ralf Bartenschlager, Centre for Infectious Diseases, Molecular Virology, Heidelberg), were cultured in DMEM supplemented with 10% (vol/vol) FCS and 1% Antibiotic-Antimycotic (Life Technologies) or RPMI 1640 medium supplemented with 10% (vol/vol) FBS, 1% penicillin/streptomycin, 2 mM glutamine, 1 mM Hepes, and 0.1 mM nonessential amino acids. Human embryonic kidney 293 T cells (HEK293T; ATCC CRL-1573 from LGC Standards (ATCC) were cultured in DMEM supplemented with 10% (vol/vol) FCS, 1% penicillin/streptomycin, and 2 mM glutamine. All cell lines were maintained at 37 °C with 5% CO_2 and were passaged by trypsinization at ∼80% confluence.

Mosquito Rearing and Parasite Production. For routine passage of blood-stage *Pb* parasites and for mosquito feedings, mice (4–6 wk; Janvier or Charles River Breeding Laboratories) were infected by i.p. injections. *Anopheles stephensi* mosquitoes were reared at 28 °C and 80% humidity under a 14-h/10-h light/dark cycle and fed on 10% (wt/vol) sucrose/*p*-aminobenzoic acid solution. Adult mosquitoes were fed on infected mice with *Pb* WT (62, 63) or mutant parasites and maintained at 21 °C and 80% humidity.

Parasite Strains. *Pb* ANKA (62) and *Pb*GFP-luc$_{con}$ (63) WT sporozoites, as well as transgenic *Pb*EXP-1compl and *Pb*EXP-1ΔC2 sporozoites, were obtained by dissection of salivary glands of infected *A. stephensi* mosquitoes bred at the Instituto de Medicina Molecular or at the Centre for Infectious Diseases in-house insectaries. After grinding, the suspension was filtered through a 70-μm cell strainer (Falcon) or centrifuged to remove mosquito debris. The *Pf* 3D7 strain was grown in 5% hematocrit at 37 °C, 5% CO_2, 5% O_2, and 90% N_2.

Generation of Transgenic Parasite Lines. To generate the *Pb*EXP-1ΔC2 parasite line, a 3′ UTR fragment was amplified by using 3′ *Pb*EXP-1for and 3′ *Pb*EXP-1rev primers (Table S3), and a 5′ fragment including the ORF without the last 93 bp of *Pb*EXP-1 was amplified with 5′ *Pb*EXP-1ORFdC2for and 5′ *Pb*EXP-1ORFdC2rev primers (Table S3) from *Pb* WT genomic DNA (gDNA) and cloned into the b3D$^+$ vector (64). A similar strategy was used to generate the *Pb*EXP-1compl parasite line. Briefly, a 5′ fragment comprising the complete *Pb*EXP-1 ORF was amplified by using the primers 5′ *Pb*EXP-1ORFdC2for and 5′ *Pb*EXP-1ORFcompl_rev (Table S3) from *Pb* WT gDNA and cloned into the b3D$^+$ vector (64) containing the 3′ UTR fragment as described above. Before transfection, the targeting vectors were linearized by using restriction enzymes KpnI and NotI. Transgenic *Pb* (62) and *Pb*GFP-Luc$_{con}$ (63) parasite lines were generated as described (65). To obtain clonal parasite populations, limited serial parasite dilutions were performed, and one parasite was administered by i.v. injection to each of 10 recipient naive NMRI mice (66). After gDNA extraction, *Pb* WT, *Pb*EXP-1ΔC2, and *Pb*EXP-1compl parasites were genotyped by using specific primers (Table S3). The deletion of the last 93 bp of the *Pb*EXP-1 ORF and the presence of the entire EXP-1 ORF in the *Pb*EXP-1compl parasite were additionally confirmed by sequencing.

Y2H Analysis. The Y2H technique was carried out according to the yeast protocol handbook and "Matchmaker Library Construction and Screening Kit" manual (Clontech) by using the yeast reporter strain AH109. *Pb*EXP-1 CT fragments were cloned into the pGBKT7 plasmid. *Pb*EXP-1 CT was used as bait to screen a rat hepatocyte cDNA library constructed with the "Make Your Own Mate & Plate Library" system (Clontech). Fourteen colonies were recovered from quadruple dropout (QDO; -Trp-Leu-Ade-His) plates. Direct interaction was confirmed by cotransformation of pGBKT7 and pGADT7-Rec plasmids containing the respective bait and prey sequences, followed by selection on QDO plates. For the generation of *Pb*EXP-1 and *Rn*ApoH binding and activation domain fusions, the respective coding regions were amplified by PCR using primers listed in Table S3, inserted into pGBKT7 and pGADT7-Rec plasmids, and sequenced.

Far Western Blot and Antibody Inhibition Assays. Huh7 cells (50,000) were infected with 30,000 *Pb* sporozoites and lysed 48 h later at 4 °C in 10 mM Tris·HCl (pH 7.4), 100 mM NaCl, 1% Triton X-100, 1 mM $NaVO_4$, 1 mM NaF, and complete EDTA-free protease inhibitors for 1 h with gentle rotation. After lysis, samples were centrifuged to remove insoluble cellular material. Sporozoite lysates were obtained from 400,000 *Pb* sporozoites treated as above. *Pb*- and *Pf*-infected red blood cell samples (3–5% parasitemia) were lysed in 0.1% saponin solution for 10 min followed by several washes in ice-cold PBS.

For far Western blotting experiments, protein lysates (30–40 μL) were separated by SDS/PAGE and blotted onto nitrocellulose membranes. The membranes were blocked in 5% (wt/vol) dried powdered milk in PBS containing 0.05% Tween 20 for 1 h or overnight at 4 °C. Blots were subsequently overlaid with or without rat serum with gentle mixing. After 4 h, the binding of ApoH was detected by using rabbit α-ApoH antibody (1:12,000; Abcam, ab108348), followed by a horseradish peroxidase (HRP)-conjugated rabbit secondary antibody (1:5,000; Jackson ImmunoResearch). A control lane on the blot was overlaid with α-*Pf*EXP-1 antibody (1:700) provided by K. Lingelbach, University of Marburg, Marburg, Germany.

Antibody inhibition assays were performed as described before, except that the membranes were overlaid for 8 h with α-*Pf*EXP-1 antibody before incubation with rat serum. ApoH binding to EXP-1 was detected by using α-ApoH antibody (1:12,000; Abcam, ab108348), followed by a HRP-conjugated rabbit secondary antibody (1:5,000; Jackson ImmunoResearch).

All antibodies were diluted in 5% (wt/vol) dried powdered milk in PBS containing 0.05% Tween 20, and nitrocellulose blots were overlaid with antibodies for 1 h at room temperature. The blots were developed by the addition of ECL substrate (Thermo Scientific Pierce), a chemiluminescent substrate to detect peroxidase activity from HRP-conjugated antibodies.

Immunoprecipitation. The pCMV-HA plasmid encoding the whole *Pb*EXP-1 CT (human codon-optimized) was obtained from Clontech. *Rn*ApoH was amplified by PCR from a rat hepatocyte cDNA library (Table S3), and the PCR product was cloned into pCMV-myc (Clontech). All constructs were analyzed by DNA sequencing and enzyme digestion. Protein expression was confirmed by Western blotting.

HEK293T cells (3×10^6 cells per plate) were transiently transfected by using FuGENE 6 (Roche Molecular Biochemicals) with expression plasmids carrying *Pb*EXP-1 (5 μg) and *Rn*ApoH (5 μg) and cultured for 48 h. They were subsequently washed with ice-cold PBS and lysed in ice-cold lysis buffer [10 mM Tris·HCl, pH 7.4, 100 mM NaCl, 1% Triton X-100, 1 mM $NaVO_4$, 1 mM NaF, and complete EDTA-free protease inhibitors]. Lysates were cleared by centrifugation, and the supernatants were incubated with α-HA antibody (Abcam, ab9110; or Sigma, H9658) at 4 °C for 2 h. Immune complexes were recovered by incubation with protein G-Sepharose beads (Amersham Biosciences) for 1 h at 4 °C. After three washes with ice-cold lysis buffer, protein complexes were dissociated from the protein G by addition of Laemmli's sample buffer and boiled for 10 min at 100 °C. Samples were then centrifuged, and the supernatant was loaded onto polyacrylamide gels. Separated proteins were transferred to nitrocellulose membranes, and immunoprecipitates were then analyzed by immunoblotting using appropriate primary antibodies (1:1,000, Clontech, α-cmyc 631206; or 1:12,000, Abcam, α-ApoH Ab 108348), followed by HRP-conjugated secondary antibodies (1:5,000; Jackson ImmunoResearch) and developed as described above.

Assessment of in Vivo *Plasmodium* Infection. For quantification of liver infection, C57BL/6 mice (6–8 wk) were injected i.v. with 10,000 *Pb* WT or *Pb*EXP-1ΔC2 sporozoites. Liver infection load was quantified after 42–46, 72, and 96 hpi by qRT-PCR analysis. To this end, whole livers were homogenized in 3 mL of denaturing solution (4 M guanidine thiocyanate, 25 mM sodium citrate, pH 7, 0.5% *N*-lauroylsarcosine, and 0.7% (vol/vol) β-mercaptoethanol in diethyl pyrocarbonate-treated water) or 4 mL of RLT buffer (Qiagen) containing 1% β-mercaptoethanol, followed by RNA extraction and qRT-PCR analysis as described.

For assessment of blood-stage infection, C57BL/6 mice (6–8 wk) were injected i.v. with 10,000 *Pb* WT or *Pb*EXP-1ΔC2 sporozoites or with 1×10^6 infected erythrocytes from these parasite lines. Parasitemia was monitored daily by examination of Giemsa-stained blood smears and was used to calculate the number of asexual blood stages in mice for each day after infection. The growth or multiplication rate was determined for each day according to the following formula: (no. of total parasites/no. of parasites injected)^1/d after infection (67, 68).

Mice were observed daily for signs of experimental cerebral malaria (ECM), including the following neurological symptoms: hemiplegia and paraplegia, ataxia, convulsion, and/or coma. Animals exhibiting signs of severe disease and mice that did not develop ECM but developed hyperparasitemia and anemia were euthanized.

siRNA-Mediated in Vitro Gene Expression Silencing. Huh7 cells (40,000) were seeded and transfected with either of three predesigned ApoH-silencer double-stranded RNAs (Table S3), by using Lipofectamine RNAimax (Life Technologies) according to the manufacturer's instructions. Thirty-six hours later, cells were infected with 10,000 luciferase-expressing *Pb* parasites. A scrambled siRNA and a siRNA targeting the SRBI (Table S3) gene were used as negative and positive controls, respectively. Down-regulation of ApoH was confirmed by either qRT-PCR or Western blot analysis using α-ApoH antibody (1:12,000; Abcam, ab108348) and HRP-coupled anti-rabbit IgG secondary antibody (1:5,000; Jackson ImmunoResearch).

Infection was assessed by immunofluorescence microscopy, qRT-PCR, or bioluminescence (Biotium). In the latter case, cell viability was assessed 44 hpi by the

CellTiter-Blue assay (Promega) according to the manufacturer's protocol, and parasite load was measured 48 hpi by using a multiplate reader Infinite M200 (Tecan).

rAAV-Mediated in Vivo Gene Expression Silencing. Self-complementary rAAV vectors expressing shRNAs against murine ApoH under a H1 promoter were generated as described (69). Targeted sense sequences for *Mm*ApoH shRNAs 176 and 725 (Table S3) were selected by using siRNA Wizard (InvivoGen), and rAAV vectors expressing nonsilencing (Ns1) shRNAs were used as controls. All rAAV vectors were produced by triple transfection of HEK293T cells (30 plates with 4×10^6 cells per shRNA) with equal amounts (14.6 μg per plate) of AAV helper plasmid encoding AAV8 capsid genes, an adenoviral helper construct and rAAV vector plasmids (70) encoding Ns1 or anti-*Mm*ApoH shRNAs. rAAV vector particles were purified by cesium chloride density gradient centrifugation (69).

For in vivo ApoH silencing, 5×10^{10} rAAV particles were administered to female C57BL/6 mice by i.v. injection. Fourteen days later, mice were infected by i.v. injection of 10,000 *Pb* WT sporozoites. Liver infection load was quantified 42 hpi by qRT-PCR.

Assessment of Gene Expression by qRT-PCR. RNA was extracted from hepatic cells or tissues by using the RNeasy Mini kit (Qiagen), and cDNA was obtained by reverse transcription (First-Strand cDNA Synthesis kit; Roche/Thermo Fisher Scientific). For quantification of infection, qRT-PCR was performed by using primers specific for *Pb* 18S rRNA. For assessment of gene silencing, ApoH-specific primers were used. Gene expression levels were normalized against mouse hypoxanthine guanine phosphoribosyltransferase (HPRT) or GAPDH by using the $\Delta\Delta C_T$ method. Primer sequences are shown in Table S3.

Immunofluorescence Microscopy. A total of 50,000 and 25,000 Huh7 cells grown on coverslips or eight-well Lab-Tek chamber slides (Nunc), respectively, were seeded 1 d before infection with 10,000 *Pb* sporozoites and fixed at the indicated time points (10, 15, 18, 21, 24, and 48 hpi) after sporozoite addition. Cells grown on coverslips were fixed with 4% (vol/vol) paraformaldehyde for 15 min, washed three times with PBS, permeabilized in 0.2% (vol/vol) saponin or Triton in PBS for 20 min, blocked for 1 h with 0.1% (vol/vol) Triton in 1% (wt/vol) BSA in PBS, and incubated with the appropriate primary antibodies in blocking buffer for 1 h at room temperature or overnight at 4 °C. Primary antibodies used were mouse monoclonal antibody 2E6 against *Pb* heat-shock protein 70 (HSP70) (1:100) (71), goat anti-UIS4 antibody (1:1,000), chicken anti–*Pb*EXP-1 antibody (1:700; provided by Volker Heussler, Institute of Cell Biology, University of Bern, Bern, Switzerland), mouse anti–*Pb*EXP-1^c antibody (1:300; raised against the CT part of *Pb*EXP-1, i.e., amino acids 103–166; see also Fig. 1*A*), and rabbit monoclonal anti-ApoH antibody (1:10; Sigma, HPA003732). After three washes with PBS, cells were incubated for 40 min with secondary antibodies diluted in blocking buffer. Nuclei were stained with DAPI or Hoechst, and coverslips were mounted onto microscope slides with Fluoromount G mounting medium (SouthernBiotech, catalog no. 0100-01).

Cells grown in Lab-Tek chamber slides were fixed with ice-cold methanol for 10 min, washed three times with 1% FCS in PBS, blocked overnight with 10% (vol/vol) FCS in PBS at 4 °C, and incubated with primary antibodies in blocking buffer for 1 h at 37 °C. Primary antibodies used were monoclonal anti-*Pb*HSP70 antibody (1:50), rat anti-*Pb*UIS4 antibody (1:300), or mouse anti–*Pb*EXP-1^c antibody (1:300). After three washes with 1% FCS in PBS, cells were incubated for 1 h at 37 °C with secondary antibodies (1:300) diluted in blocking buffer. Nuclei were stained with DAPI, followed by addition of 50% (vol/vol) glycerol in PBS and sealing with a coverslip.

All images were acquired on Zeiss wide-field Fluorescence Axiovert 200M or on Zeiss LSM 510 META or Zeiss LSM 710 confocal laser point-scanning microscopes. Image analysis was performed by using the LSM image browser and ImageJ.

Analysis of ApoH–EXP-1 Colocalization and ApoH Accumulation. Confocal microscopy images were obtained by sequential scanning for each channel to eliminate the cross-talk of chromophores. The background was corrected by using the threshold value for all channels. ApoH–EXP-1 colocalization was quantified by using the "co-localization highlighter" command in ImageJ software. The colocalizing pixels identified were represented as a percentage of the total EXP-1 signal. The accumulation of ApoH was assessed by using ImageJ by calculating the difference between the total ApoH signal inside the EEF and the ApoH signal in an area of the same size and shape outside the EEF and normalized to the EEF area.

Quantification of in Vitro Merosome Formation. Huh7 cells (25,000) were seeded in eight-well Lab-Tek chamber slides (Nunc) and infected 24 h later with 40,000 *Pb* WT or *Pb*EXP-1ΔC2 sporozoites, and merosome formation was quantified at 48, 65, and 72 hpi. At the indicated time points, culture supernatants were collected and centrifuged at $100 \times g$ for 5 min at room temperature. The supernatants were carefully removed, and merosomes in the pellet were counted by using a hemocytometer to estimate the total number of merosomes per well.

Statistical Analyses. Statistical significance was assessed by using the unpaired *t* test, two-tailed nonparametric Mann–Whitney test, one-way ANOVA, and Dunnett's multiple comparison test, or log-rank (Mantel–Cox) test. Values of $P < 0.05$ were deemed statistically significant (in the figures, $*P < 0.05$; $**P < 0.01$; and $***P < 0.001$). All statistical analyses were performed by using the GraphPad Prism (Version 5.0) or SigmaPlot (Version 13) software.

ACKNOWLEDGMENTS. We thank Jennifer Schahn, Miriam Reinig, Filipa Teixeira, and Ana Parreira for mosquito breeding; Priyanka Fernandes, Franziska Hentzschel, Jessica Kehrer, and Mirko Singer for both expert technical assistance and critical discussions; and Anne-Kathrin Herrmann and Liesa-Marie Schreiber for technical assistance. Anti–*Pb*EXP-1 antiserum was kindly provided by Volker Heussler, and α-*Pf*EXP-1 antibody was kindly provided by the laboratory of Prof. K. Lingelbach. This study was supported by German Research Foundation (DFG) Grants SPP 1580 (to A.-K.M.) and SFB1129/TP2 (to A.-K.M. and D.G.); and Fundação para a Ciência e Tecnologia, Portugal (FCT-PT) Grant PTDC/SAUMIC/117060/2010 (to M.P.). C.S.e.C. and M.S.-V. were supported by FCT-PT Grants SFRH/BPD/45201/2008 and PD/BD/105838/2014, respectively. B.N. received a HBIGS doctoral fellowship (DFG Fonds 26249/7808421). M.P. was supported by a FCT-PT Investigador FCT 2013 fellowship.

1. Prudêncio M, Rodriguez A, Mota MM (2006) The silent path to thousands of merozoites: The *Plasmodium* liver stage. *Nat Rev Microbiol* 4(11):849–856.
2. Rodrigues T, Prudêncio M, Moreira R, Mota MM, Lopes F (2012) Targeting the liver stage of malaria parasites: A yet unmet goal. *J Med Chem* 55(3):995–1012.
3. Amino R, et al. (2006) Quantitative imaging of *Plasmodium* transmission from mosquito to mammal. *Nat Med* 12(2):220–224.
4. Frevert U, et al. (2005) Intravital observation of *Plasmodium berghei* sporozoite infection of the liver. *PLoS Biol* 3(6):e192.
5. Mota MM, et al. (2001) Migration of *Plasmodium* sporozoites through cells before infection. *Science* 291(5501):141–144.
6. Lingelbach K, Joiner KA (1998) The parasitophorous vacuole membrane surrounding *Plasmodium* and *Toxoplasma*: An unusual compartment in infected cells. *J Cell Sci* 111(Pt 11):1467–1475.
7. Albuquerque SS, et al. (2009) Host cell transcriptional profiling during malaria liver stage infection reveals a coordinated and sequential set of biological events. *BMC Genomics* 10:270–282.
8. Itoe MA, et al. (2014) Host cell phosphatidylcholine is a key mediator of malaria parasite survival during liver stage infection. *Cell Host Microbe* 16(6):778–786.
9. Meireles P, *et al*. (2016) GLUT1-mediated glucose uptake plays a crucial role during *Plasmodium* hepatic infection. *Cell Microbiol*, 10.1111/cmi.12646 {Epub ahead of print].
10. Allary M, Lu JZ, Zhu L, Prigge ST (2007) Scavenging of the cofactor lipoate is essential for the survival of the malaria parasite *Plasmodium falciparum*. *Mol Microbiol* 63(5):1331–1344.
11. Tarun AS, et al. (2008) A combined transcriptome and proteome survey of malaria parasite liver stages. *Proc Natl Acad Sci USA* 105(1):305–310.
12. Deschermeier C, et al. (2012) Mitochondrial lipoic acid scavenging is essential for *Plasmodium berghei* liver stage development. *Cell Microbiol* 14(3):416–430.
13. Spielmann T, Montagna GN, Hecht L, Matuschewski K (2012) Molecular make-up of the *Plasmodium* parasitophorous vacuolar membrane. *Int J Med Microbiol* 302(4-5):179–186.
14. Bano N, Romano JD, Jayabalasingham B, Coppens I (2007) Cellular interactions of *Plasmodium* liver stage with its host mammalian cell. *Int J Parasitol* 37(12):1329–1341.
15. Lopes da Silva M, et al. (2012) The host endocytic pathway is essential for *Plasmodium berghei* late liver stage development. *Traffic* 13(10):1351–1363.
16. Grützke J, et al. (2014) The spatiotemporal dynamics and membranous features of the *Plasmodium* liver stage tubovesicular network. *Traffic* 15(4):362–382.
17. Thieleke-Matos C, et al. (2014) Host PI(3,5)P2 activity is required for *Plasmodium berghei* growth during liver stage infection. *Traffic* 15(10):1066–1082.
18. Prado M, et al. (2015) Long-term live imaging reveals cytosolic immune responses of host hepatocytes against *Plasmodium* infection and parasite escape mechanisms. *Autophagy* 11(9):1561–1579.
19. Thieleke-Matos C, et al. (2016) Host cell autophagy contributes to *Plasmodium* liver development. *Cell Microbiol* 18(3):437–450.
20. MacKellar DC, Vaughan AM, Aly AS, DeLeon S, Kappe SH (2011) A systematic analysis of the early transcribed membrane protein family throughout the life cycle of *Plasmodium yoelii*. *Cell Microbiol* 13(11):1755–1767.
21. Matuschewski K, et al. (2002) Infectivity-associated changes in the transcriptional repertoire of the malaria parasite sporozoite stage. *J Biol Chem* 277(44):41948–41953.
22. Kaiser K, Matuschewski K, Camargo N, Ross J, Kappe SH (2004) Differential transcriptome profiling identifies *Plasmodium* genes encoding pre-erythrocytic stage-specific proteins. *Mol Microbiol* 51(5):1221–1232.
23. Mueller AK, et al. (2005) *Plasmodium* liver stage developmental arrest by depletion of a protein at the parasite-host interface. *Proc Natl Acad Sci USA* 102(8):3022–3027.

24. Mueller AK, Labaied M, Kappe SH, Matuschewski K (2005) Genetically modified *Plasmodium* parasites as a protective experimental malaria vaccine. *Nature* 433(7022): 164–167.
25. Mikolajczak SA, Jacobs-Lorena V, MacKellar DC, Camargo N, Kappe SH (2007) L-FABP is a critical host factor for successful malaria liver stage development. *Int J Parasitol* 37(5):483–489.
26. Vignali M, et al. (2008) Interaction of an atypical *Plasmodium falciparum* ETRAMP with human apolipoproteins. *Malar J* 7:211–218.
27. Garcia J, et al. (2009) Synthetic peptides from conserved regions of the *Plasmodium falciparum* early transcribed membrane and ring exported proteins bind specifically to red blood cell proteins. *Vaccine* 27(49):6877–6886.
28. Hall R, et al. (1983) Antigens of the erythrocytes stages of the human malaria parasite *Plasmodium falciparum* detected by monoclonal antibodies. *Mol Biochem Parasitol* 7(3):247–265.
29. Hope IA, Mackay M, Hyde JE, Goman M, Scaife J (1985) The gene for an exported antigen of the malaria parasite *Plasmodium falciparum* cloned and expressed in *Escherichia coli*. *Nucleic Acids Res* 13(2):369–379.
30. Coppel RL, et al. (1985) A blood stage antigen of *Plasmodium falciparum* shares determinants with the sporozoite coat protein. *Proc Natl Acad Sci USA* 82(15): 5121–5125.
31. Simmons D, Woollett G, Bergin-Cartwright M, Kay D, Scaife J (1987) A malaria protein exported into a new compartment within the host erythrocyte. *EMBO J* 6(2):485–491.
32. Sanchez GI, Rogers WO, Mellouk S, Hoffman SL (1994) *Plasmodium falciparum*: Exported protein-1, a blood stage antigen, is expressed in liver stage parasites. *Exp Parasitol* 79(1):59–62.
33. Charoenvit Y, et al. (1995) *Plasmodium yoelii*: 17-kDa hepatic and erythrocytic stage protein is the target of an inhibitory monoclonal antibody. *Exp Parasitol* 80(3): 419–429.
34. Günther K, et al. (1991) An exported protein of *Plasmodium falciparum* is synthesized as an integral membrane protein. *Mol Biochem Parasitol* 46(1):149–157.
35. Ansorge I, Paprotka K, Bhakdi S, Lingelbach K (1997) Permeabilization of the erythrocyte membrane with streptolysin O allows access to the vacuolar membrane of *Plasmodium falciparum* and a molecular analysis of membrane topology. *Mol Biochem Parasitol* 84(2):259–261.
36. Currà C, et al. (2012) Erythrocyte remodeling in *Plasmodium berghei* infection: The contribution of SEP family members. *Traffic* 13(3):388–399.
37. Spielmann T, Gardiner DL, Beck HP, Trenholme KR, Kemp DJ (2006) Organization of ETRAMPs and EXP-1 at the parasite-host cell interface of malaria parasites. *Mol Microbiol* 59(3):779–794.
38. Hanson KK, et al. (2013) Torins are potent antimalarials that block replenishment of *Plasmodium* liver stage parasitophorous vacuole membrane proteins. *Proc Natl Acad Sci USA* 110(30):E2838–E2847.
39. Maier AG, et al. (2008) Exported proteins required for virulence and rigidity of *Plasmodium falciparum*-infected human erythrocytes. *Cell* 134(1):48–61.
40. Bozdech Z, et al. (2003) The transcriptome of the intraerythrocytic developmental cycle of *Plasmodium falciparum*. *PLoS Biol* 1(1):E5.
41. Le Roch KG, et al. (2004) Global analysis of transcript and protein levels across the *Plasmodium falciparum* life cycle. *Genome Res* 14(11):2308–2318.
42. Lisewski AM, et al. (2014) Supergenomic network compression and the discovery of EXP1 as a glutathione transferase inhibited by artesunate. *Cell* 158(4):916–928.
43. Prudêncio M, Mota MM, Mendes AM (2011) A toolbox to study liver stage malaria. *Trends Parasitol* 27(12):565–574.
44. Ploemen IH, et al. (2009) Visualisation and quantitative analysis of the rodent malaria liver stage by real time imaging. *PLoS One* 4(11):e7881.
45. Gao GP, et al. (2002) Novel adeno-associated viruses from rhesus monkeys as vectors for human gene therapy. *Proc Natl Acad Sci USA* 99(18):11854–11859.
46. Thomas CE, Storm TA, Huang Z, Kay MA (2004) Rapid uncoating of vector genomes is the key to efficient liver transduction with pseudotyped adeno-associated virus vectors. *J Virol* 78(6):3110–3122.
47. Nakai H, et al. (2005) Unrestricted hepatocyte transduction with adeno-associated virus serotype 8 vectors in mice. *J Virol* 79(1):214–224.
48. Grimm D, Pandey K, Nakai H, Storm TA, Kay MA (2006) Liver transduction with recombinant adeno-associated virus is primarily restricted by capsid serotype not vector genotype. *J Virol* 80(1):426–439.
49. Pfander C, et al. (2011) A scalable pipeline for highly effective genetic modification of a malaria parasite. *Nat Methods* 8(12):1078–1082.
50. Ishino T, et al. (2009) LISP1 is important for the egress of *Plasmodium berghei* parasites from liver cells. *Cell Microbiol* 11(9):1329–1339.
51. Orito Y, et al. (2013) Liver-specific protein 2: A *Plasmodium* protein exported to the hepatocyte cytoplasm and required for merozoite formation. *Mol Microbiol* 87(1): 66–79.
52. Ingmundson A, Nahar C, Brinkmann V, Lehmann MJ, Matuschewski K (2012) The exported *Plasmodium berghei* protein IBIS1 delineates membranous structures in infected red blood cells. *Mol Microbiol* 83(6):1229–1243.
53. Matz JM, et al. (2015) The *Plasmodium berghei* translocon of exported proteins reveals spatiotemporal dynamics of tubular extensions. *Sci Rep* 5:12532–12545.
54. Averna M, et al. (1997) Liver is not the unique site of synthesis of beta 2-glycoprotein I (apolipoprotein H): Evidence for an intestinal localization. *Int J Clin Lab Res* 27(3): 207–212.
55. Chamley LW, Allen JL, Johnson PM (1997) Synthesis of beta2 glycoprotein 1 by the human placenta. *Placenta* 18(5-6):403–410.
56. Steinkasserer A, Estaller C, Weiss EH, Sim RB, Day AJ (1991) Complete nucleotide and deduced amino acid sequence of human beta 2-glycoprotein I. *Biochem J* 277(Pt 2): 387–391.
57. de Groot PG, Meijers JC (2011) β(2)-Glycoprotein I: Evolution, structure and function. *J Thromb Haemost* 9(7):1275–1284.
58. Lozier J, Takahashi N, Putnam FW (1984) Complete amino acid sequence of human plasma beta 2-glycoprotein I. *Proc Natl Acad Sci USA* 81(12):3640–3644.
59. Zhang C, et al. (2010) Detection of serum beta(2)-GPI-Lp(a) complexes in patients with systemic lupus erythematosus. *Clinica Chimica Acta* 411(5-6):395–399.
60. De Groot PG, Meijers JC, Urbanus RT (2012) Recent developments in our understanding of the antiphospholipid syndrome. *Int J Lab Hematol* 34(3):223–231.
61. Wang SX, Cai GP, Sui SF (1998) The insertion of human apolipoprotein H into phospholipid membranes: A monolayer study. *Biochem J* 335(Pt 2):225–232.
62. Hall N, et al. (2005) A comprehensive survey of the *Plasmodium* life cycle by genomic, transcriptomic, and proteomic analyses. *Science* 307(5706):82–86.
63. Janse CJ, et al. (2006) High efficiency transfection of *Plasmodium berghei* facilitates novel selection procedures. *Mol Biochem Parasitol* 145(1):60–70.
64. Silvie O, Goetz K, Matuschewski K (2008) A sporozoite asparagine-rich protein controls initiation of *Plasmodium* liver stage development. *PLoS Pathog* 4(6):e1000086.
65. Janse CJ, Ramesar J, Waters AP (2006) High-efficiency transfection and drug selection of genetically transformed blood stages of the rodent malaria parasite *Plasmodium berghei*. *Nat Protoc* 1(1):346–356.
66. Thathy V, Ménard R (2002) Gene targeting in *Plasmodium berghei*. *Methods Mol Med* 72:317–331.
67. Klug D, Mair GR, Frischknecht F, Douglas RG (2016) A small mitochondrial protein present in myzozoans is essential for malaria transmission. *Open Biol* 6(4):160034.
68. Spaccapelo R, et al. (2010) Plasmepsin 4-deficient *Plasmodium berghei* are virulence attenuated and induce protective immunity against experimental malaria. *Am J Pathol* 176(1):205–217.
69. Grimm D, et al. (2006) Fatality in mice due to oversaturation of cellular microRNA/short hairpin RNA pathways. *Nature* 441(7092):537–541.
70. Börner K, et al. (2013) Robust RNAi enhancement via human Argonaute-2 overexpression from plasmids, viral vectors and cell lines. *Nucleic Acids Res* 41(21):e199.
71. Tsuji M, Mattei D, Nussenzweig RS, Eichinger D, Zavala F (1994) Demonstration of heat-shock protein 70 in the sporozoite stage of malaria parasites. *Parasitol Res* 80(1): 16–21.
72. Rodrigues CD, et al. (2008) Host scavenger receptor SR-BI plays a dual role in the establishment of malaria parasite liver infection. *Cell Host Microbe* 4(3):271–282.